

Volumetric, dielectric, calorimetric and X-ray studies of smectogenic 10PBO8 at atmospheric and elevated pressures

C. M. Roland^a, D. Fragiadakis^a, R. Bogoslovov^a, S. Urban^{b*}, R. Dąbrowski^c, M. Tykarska^c, N. Osiecka^d and J. Czub^e

^aChemistry Division, Code 6120, Naval Research Laboratory, Washington, USA; ^bInstitute of Physics, Jagiellonian University, Krakow, Poland; ^cInstitute of Chemistry, Military University of Technology, Warsaw, Poland; ^dInstitute of Nuclear Physics of the Polish Academy of Sciences, Krakow, Poland; ^eFaculty of Physics and Applied Computer Sciences, AGH, Krakow, Poland

(Received 3 April 2012; final version received 26 April 2012)

The synthesis and pressure–volume–temperature (PVT), differential thermal analysis (DTA), dielectric and X-ray diffraction data of 2-(4-octylcarbonyloxyphenyl)-5-decylpyrimidine (10PBO8) are presented. The substance exhibits two crystalline and smectic C (SmC) phases on heating and a SmC–monotropic crystalline smectic B (SmB_{cr}) SmB_{cr}–crystal sequence of phase transitions on cooling. Above ca. 15 MPa, the SmB_{cr} phase becomes enantiotropic (reversible polymorphism). The phase behaviour and molecular dynamics in the liquid crystalline phases are analysed and discussed, with the conformational component of the total entropy for the SmC–isotropic liquid transition estimated. We also calculate from the PVT results the potential parameter characterising the steepness of the interaction potential.

Keywords: smectogen; high-pressure; phase diagram; X-ray; potential parameter

1. Introduction

Studies combining different experimental methods are best for understanding the physical properties of materials. This is especially the case for complex chemical structures, such as glass-forming liquids, polymers and liquid crystals (LCs). The phase transitions and the dynamics in the different phases, the thermodynamic equation of state $V(P,T)$ and the relationships between these properties are central aspects of the behaviour. Interesting in this regard is that, despite differences in the molecular arrangements between glass-forming liquids and LCs, several striking analogies in their properties have been reported [1, 2].

Studies using elevated pressure have been carried out for dozens of calamitic liquid crystals exhibiting various polymorphisms (for reviews see [1–8]). Many aspects of the LC state were investigated and of interest herein is that the phase behaviour appears to be very sensitive to the applied pressure. Typically, $\partial T/\partial P$ is larger along the clearing line than for melting, which results in a broadening of the LC phase region with increasing pressure. The phase boundaries can be represented by quadratic polynomials in T and P . Often, freezing of a LC phase leads to super-cooling (or ‘super-pressing’), but such metastable states are not observed when traversing the clearing line. An interesting feature of some smectogenic LCs subjected to pressure (and temperature) is the induction of less ordered LC phases [5, 9–13]. The clearing line splits,

with a triple point emerging that separates into three distinct phases. On the other hand, in some cases the smectic phase is suppressed by pressure [5, 14].

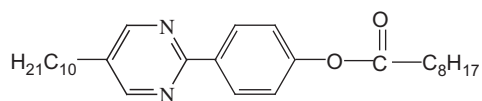
From the experimental $V(P,T)$, dynamic properties (relaxation time τ , viscosity, diffusion constant, etc.) can be calculated for isobaric, isothermal and isochoric conditions [1, 2, 4, 8, 15–17]. This enables the determination, via the thermodynamic scaling procedure, $\tau = f(TV^\gamma)$, of the interaction parameter γ characterizing the steepness of the intermolecular potential [15–17]. According to the mean-field theory of liquid crystals [18], the product $T_c V_c^\Gamma$ is constant, where T_c and V_c refer to the respective temperature and specific volume along the pressure-dependent phase boundary, and the thermodynamic potential parameter Γ is defined as

$$\Gamma = - \left(\frac{d \log T_c}{d \log V_c} \right)_P. \quad (1)$$

Originally, Equation (1) was derived for the nematic–isotropic phase boundary, but it has been employed for analyses of other transitions [19, 20]. The possible equivalence of the two potential parameters, γ and Γ , was discussed in [1, 2, 17].

In the present paper we report results for a newly synthesised LC compound, 2-(4-octylcarbonyloxyphenyl)-5-decylpyrimidine (10PBO8, $M = 452 \text{ g mol}^{-1}$),

*Corresponding author. Email: ufurban@cyf-kr.edu.pl



which exhibits the smectic C–isotropic phase transition (SmC–Iso) [21]. Calorimetric and polarising thermomicroscopy studies show another, monotropic, LC phase on cooling the sample. Herein, the phase behaviour is studied in detail, using measurements carried out as a function of temperature, pressure and volume. The rotational motion of 10PBO8 molecules about their short axes (flip-flop motion) is followed by dielectric spectroscopy. The available frequency range, however, only allows spectra to be measured for the SmC phase. From PVT data the interaction parameter Γ for the SmC–Iso boundary is obtained, along with estimates of the configurational entropy contribution to the total entropy change at the clearing transition.

2. Experimental

2.1 Synthesis

The substance was synthesised at the Institute of Chemistry, Military University of Technology, Warsaw, Poland. The method used the common procedure of forming a pyrimidine ring via condensation of formyl enamine with amidine [22], but modified as presented in Scheme 1. Formyl enamine (A), prepared in a few stages from dodecanal, was refluxed in propanol with benzyloxyamidine (B) in the presence of sodium propanolate as a base. The obtained 5-decyl-2-(4-benzyloxyphenyl)pyrimidine (C) was then treated by hydrogen in the presence of Pd/C catalyst, to yield the corresponding phenol (D), which was in turn converted to 10PBO8 via reaction with nonanoic chloride.

The structures of the intermediate and final products were confirmed by infrared (IR), proton nuclear magnetic resonance (^1H NMR), and gas chromatography/mass spectrometry-electrospray ionisation (GC/MS-EI) (Agilent 6890 N) with mass detection (Agilent MSD 5973 N).

2.2 PVT measurements

Pressure–volume–temperature (PVT) measurements utilised a Gnomix instrument [23]. The change in specific volume was measured during temperature ramps at 0.5 K min^{-1} for various pressures up to 200 MPa, with the density at 0.1 MPa determined from the buoyancy.

2.3 DTA measurements

The experimental set-up was described in [24]. Two thermocouples (indium capsules) were positioned at the bottom of the high-pressure vessel, one containing ca. 0.1 mL of the sample and the other empty. Argon was used as the pressure medium; gas leakage limited these measurements to 90°C .

2.4 Dielectric measurements

For dielectric measurements the 10PBO8 was contained between circular electrodes (15 mm diameter) with a 0.2 mm PTFE spacer to maintain a constant thickness. Spectra were measured with a Novocontrol Alpha analyser.

3. Results

Figure 1 shows the DTA traces recorded during heating and cooling at 5 K min^{-1} . The transition temperatures (onset points in Celsius) and corresponding transition enthalpies (in parentheses; kJ mol^{-1}) are:

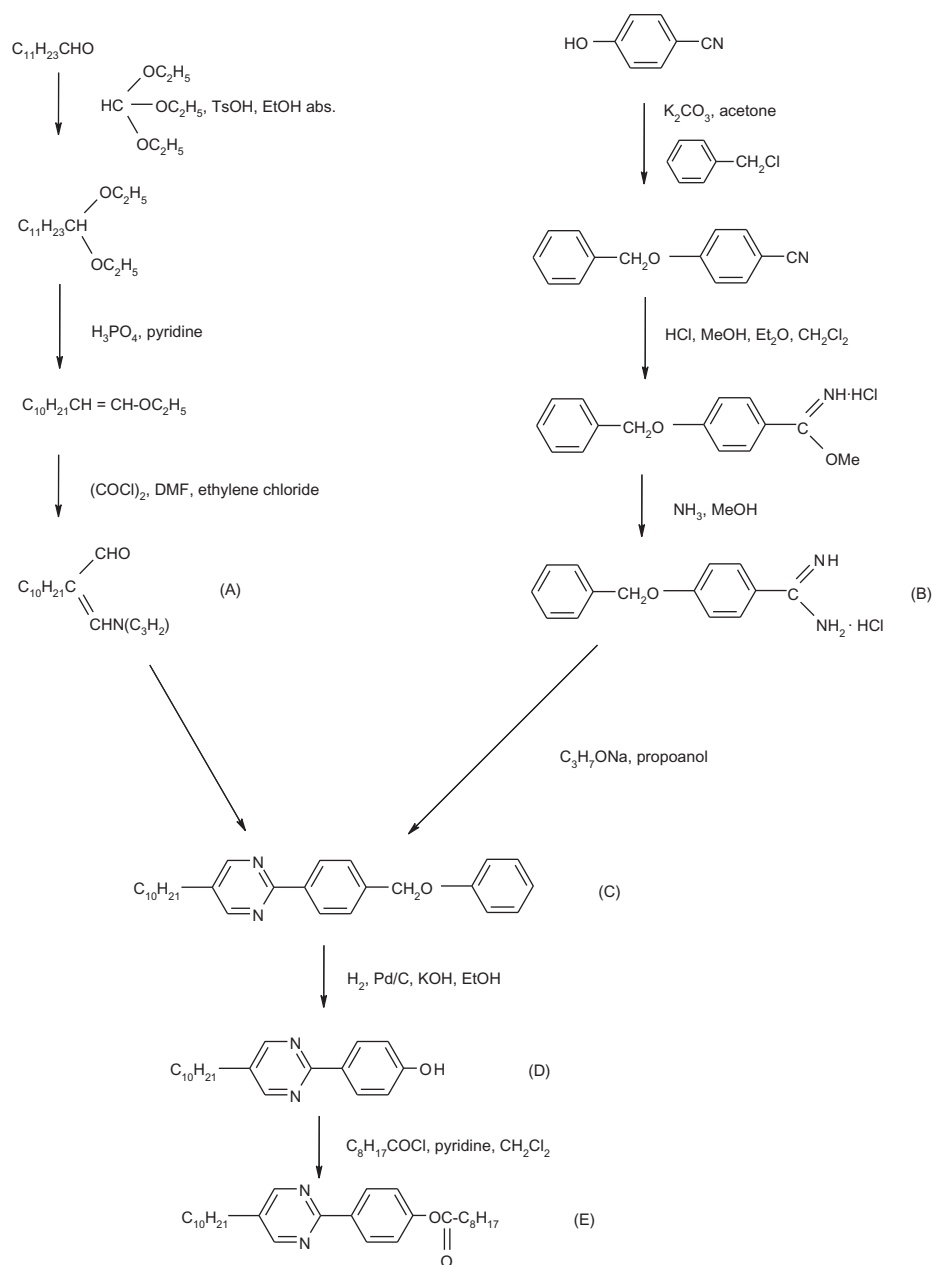
$$\begin{aligned} \text{heating: } & \text{Cr II} - 34.7 (18.5) - \text{Cr I} - 47.2 (22.4) - \\ & \text{SmC} - 64.6 (9.4) - \text{I} \\ \text{cooling: } & \text{I} - 66.0 (8.7) - \text{SmC} - 48.1 (1.97) - \text{SmX} - \\ & 30.2 (37.9) \text{Cr II.} \end{aligned}$$

The nature of the SmX phase is discussed below.

Figure 2 shows the isobaric $V(T)$ data, with the phase transitions evident as step changes in the specific volume. For each isobar the monotropic SmX phase appears above 10 MPa. Phase transitions observed on heating are marked in the figure by solid lines.

Representative DTA traces recorded at 1 K min^{-1} rates are shown in Figure 3. Above 15 MPa, the SmC–SmX transition is observed during both heating and cooling, with no noticeable super-cooling effect. It was confirmed that on the cooling the monotropic SmX phase transforms directly to the Cr II phase, and when following with immediate heating of the sample at fixed pressure the Cr II–Cr I–SmX–SmC–Iso phase sequence is recovered with comparable enthalpy changes.

The dielectric spectra show the relaxation process connected with longitudinal (flip-flop) motion in the SmC phase only (Figure 4(a)). There is also a strong dc-conductivity contribution at low frequencies due to ionic impurities. Figure 4(b) shows the real part of the permittivity measured at a fixed frequency during heating and cooling. At the SmC–SmX transition on cooling, the permittivity increases because of the orthogonal position of the molecular long axis with



Scheme 1. Synthetic route of 10PBO8.

respect to the layers in the SmX phase; however, the corresponding relaxation process is shifted to much lower frequencies (similar to other LC substances with liquid-like and solid-like phases [25]) and becomes masked by the conductivity. The abrupt decrease of the permittivity upon crystallisation indicates cessation of the molecular motions.

3.1 Identification of the SmX phase

The small enthalpy change and increase of the permittivity accompanying the SmC–SmX transition indicate

a smectogenic character of the X phase. In order to identify this phase, three types of experiments were conducted, polarising microscopy, the miscibility method and X-ray diffraction.

Polarising microscopy gave the textures shown in Figure 5. A comparison with standard textures [26] reveals that the texture on the left is typical for a SmC phase, whereas the one on the right resembles a SmE or SmB phase.

Mixing studies were used to construct the phase diagram by the method of [27]. The compound 4,4'-diheptylbiphenyl (7BB7) with well separated SmE

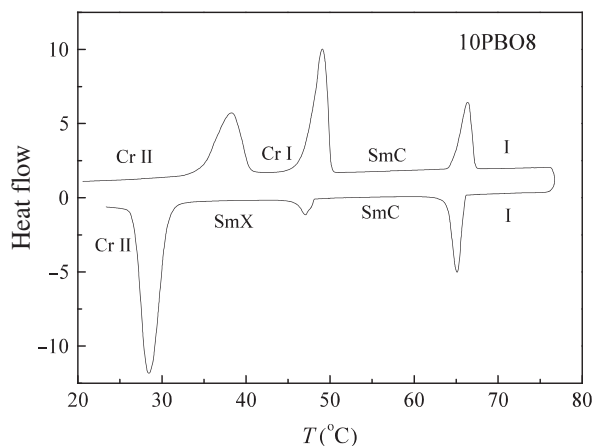


Figure 1. DSC traces of heating and cooling of the 10PBO8 sample.

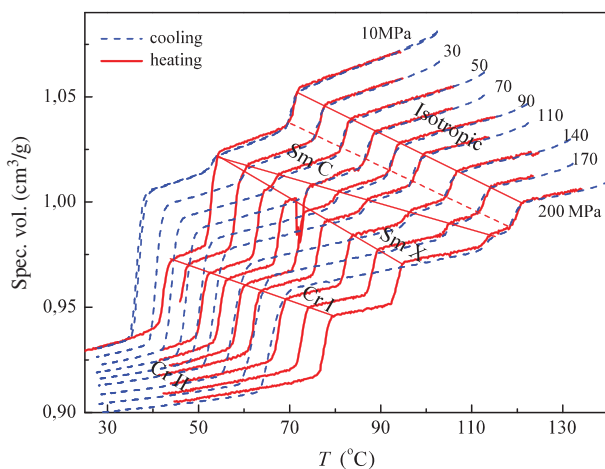


Figure 2. Isobaric data for 10PBO8 on heating (solid lines) and cooling (dashed lines). The discontinuities in volume correspond to the phase transitions (indicated by lines for the heating runs).

(19.5°C) SmE' (35.1°C) SmB_{cr} (61°C) isotropic phases [28] was used for this purpose. The smectic X phase of 10PBO8 is miscible with the SmB_{cr} phase of compound 7BB7 (Figure 6). A homeotropic texture was obtained with the use of the surfactant acetyl trimethylammonium bromide (CTAB). The microscopic texture becomes darker during cooling through the transition. Both these observations are consistent with the smectic X phase being an orthogonal SmB_{cr} phase.

X-Ray diffraction patterns, obtained by the method in [29, 30], are displayed in Figure 7. In the SmC phase a sharp peak (001) close to the incident beam and a broad maximum around $2\theta \approx 20^\circ$ were detected (Figure 7(a)). After cooling the sample to the SmX phase, a pronounced peak is observed, typical

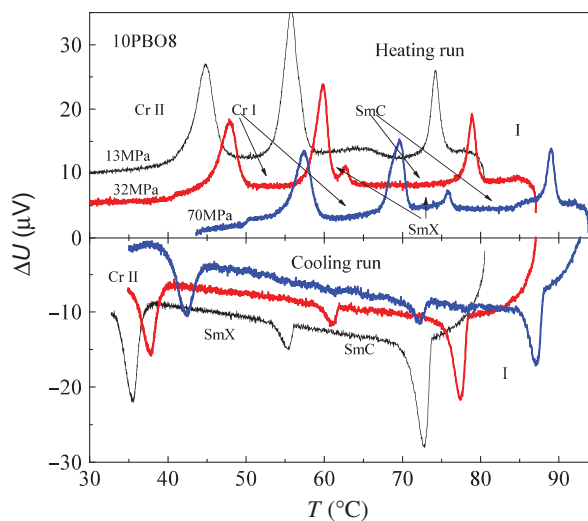


Figure 3. DTA traces at three pressures obtained on heating (upper) and cooling (lower).

for the SmB_{cr} phase [28, 31]. However, as seen in the right inset to Figure 7(a), there is a small splitting of this peak, which increases slightly on lowering temperature. Because this splitting is significantly smaller than observed for typical SmE phases [28–31], its presence in 10PBO8 may reflect interlayer ordering of the molecules [32].

Several Bragg reflections were observed in the two crystalline phases on heating (Figure 7(b)). The diffraction patterns for the two crystal forms differ considerably. Due to the limited angular range of the data, the type of the crystal structures cannot be identified, especially for the Cr II having lower symmetry. Figure 7(c) shows the X-ray patterns at 33°C for heating and cooling. Clearly, the SmB_{cr} phase transforms directly on cooling to the Cr II phase, consistent with the DTA (Figure 1) and PVT (Figure 2) results.

A strong (001) reflection was observed in all phases of 10PBO8, although in the Cr II phase it is only seen during cooling (Figure 7(c)). From this reflection we calculate the $d(001)$ spacing, corresponding to the layer thickness in the LC phases. Figure 7(d) shows stepwise changes in d at the phase transitions. Taking the value in the SmB_{cr} phase as the molecular length, which correlates well with the value of 33.5 Å estimated using HyperChem (HyperCube Inc.), we estimate the tilt angle in the SmC phase to be about 20°.

4. Discussion

4.1 P–T phase diagram

From the PVT and DTA measurements (Figure 2 and Figure 3), the T – P phase diagram can be constructed

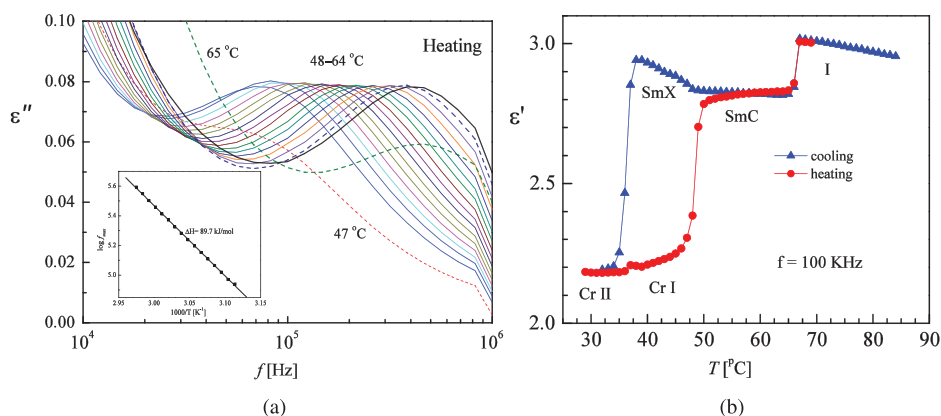


Figure 4. Dielectric spectra for 10PBO8 at 0.1 MPa: (a) isothermal loss versus frequency for increasingly higher temperatures (1 K increments). Inset shows the Arrhenius plot of the frequency of the loss maximum. The rise in ϵ'' at low frequency reflects dc-conductivity. (b) Temperature dependence of the static permittivity measured on heating and cooling.

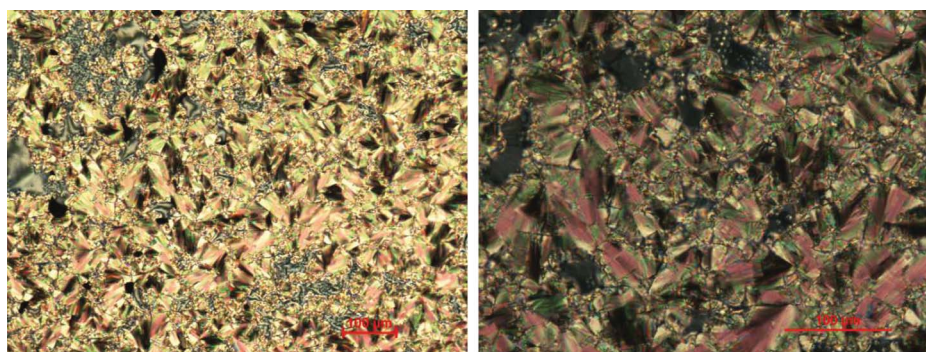


Figure 5. Textures observed at 52°C (left) and at 44°C (right) on cooling the 10PBO8 sample.

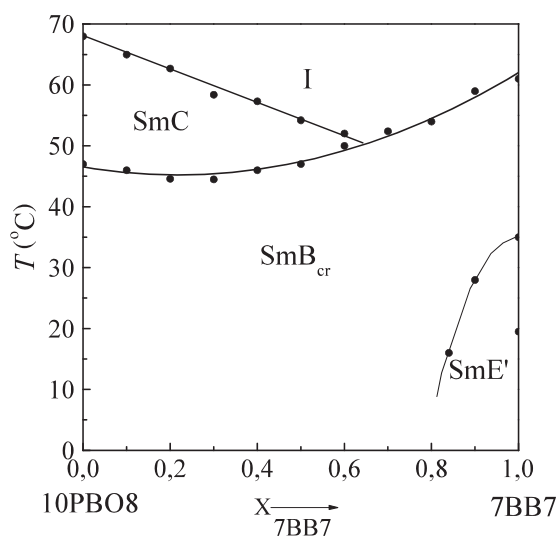


Figure 6. Phase diagrams of bi-component mixture of 10PBO8 and 7BB7.

(Figure 8). Only transitions observed during heating were considered. Agreement between both sets of data is good, especially for the $\text{SmB}_{\text{cr}}\text{-SmC}$ and

$\text{SmC}\text{-Iso}$ transitions. Because the range of the P and T variations is broader for the PVT experiment, these are analysed in more detail.

Figure 9 shows the changes in molar volume ΔV at various transitions as a function of pressure. For the $\text{Cr I}\text{-SmB}_{\text{cr}}$ phase change, ΔV diminishes with pressure; the same effect is observed for the $\text{SmB}_{\text{cr}}\text{-Cr II}$ transition on cooling. Moreover, for the latter, the change in molar volume is comparable to the sum of the ΔV accompanying the $\text{Cr I}\text{-SmB}_{\text{cr}}$ and $\text{Cr I}\text{-Cr II}$ transitions. This corroborates the conclusion derived from a comparison of the transition enthalpies and from the X-ray experiments (Figure 7(c)): on cooling one solid phase (Cr I) disappears. (Note that the transition enthalpy and volume are related by the Clausius-Clapeyron formula, $T_{tr}(\Delta V/\Delta H)_{tr} = (\partial T/\partial P)_{tr}$.)

The SmB_{cr} phase appears as monotropic at atmospheric pressure becomes enantiotropic above about 15 MPa. The temperature range of this phase broadens considerably with pressure, whereas the SmC phase shows the opposite tendency, and likely disappears entirely above ca. 345 MPa and 147°C. The quadratic

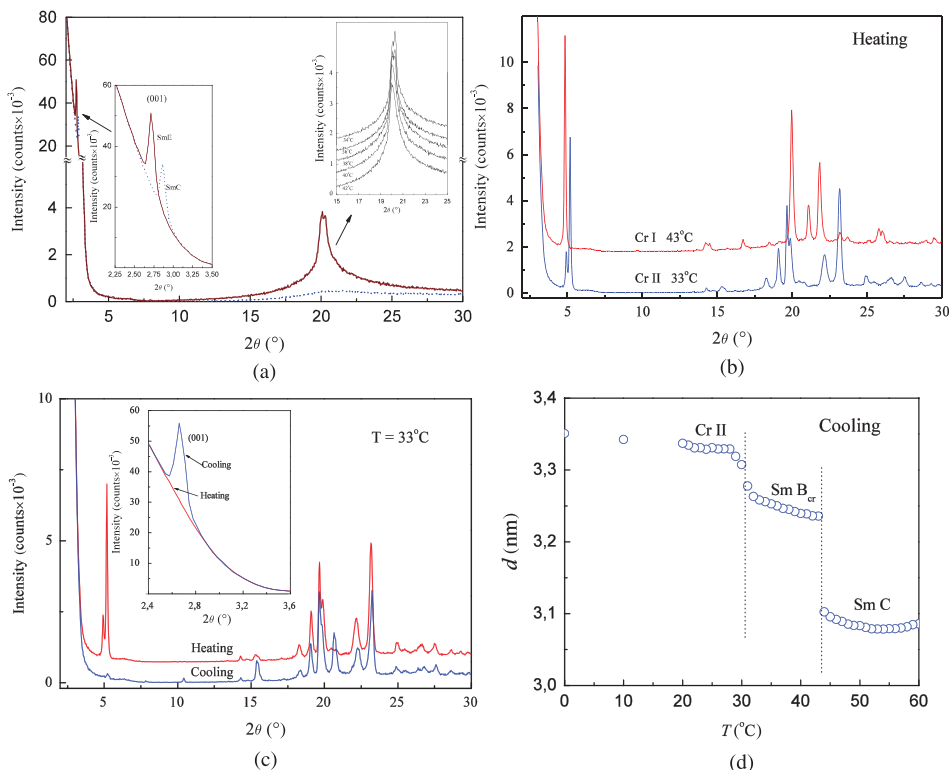


Figure 7. X-Ray patterns for different phases of 10PBO8 in the range of $2\theta = 2-30^\circ$. (a) Comparison of the patterns the SmC and SmX phases. Left inset shows the (001) reflection on an expanded scale; right inset is the reflection at $\sim 22^\circ$ at several temperatures. (b) Comparison of the diffraction patterns for two crystalline phases on heating. (c) Diffraction patterns at a given temperature reached by heating and by cooling. The (001) reflection is prominent only during cooling; see inset. (d) Lattice spacing $d(001)$ versus temperature in particular phases.

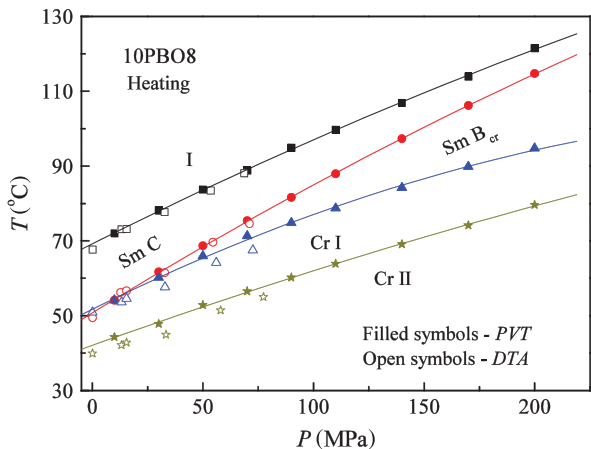


Figure 8. T - P phase diagram for 10PBO8 from PVT and DTA experiments. The lines are quadratic polynomial fits to the PVT data.

polynomial fits to the PVT data in Figure 8 (T in $^\circ\text{C}$, P in MPa):

$$\begin{aligned} \text{SmC-I} \quad T &= 68.49 + 0.311P - 2.42 \times 10^{-4} P^2 \\ \text{SmB}_{\text{cr}}\text{-SmC} \quad T &= 50.10 + 0.378P - 2.84 \times 10^{-4} P^2 \\ \text{Cr I-SmB}_{\text{cr}} \quad T &= 51.34 + 0.301P - 4.37 \times 10^{-4} P^2 \\ \text{Cr II-Cr I} \quad T &= 41.04 + 0.233P - 2.14 \times 10^{-4} P^2. \end{aligned}$$

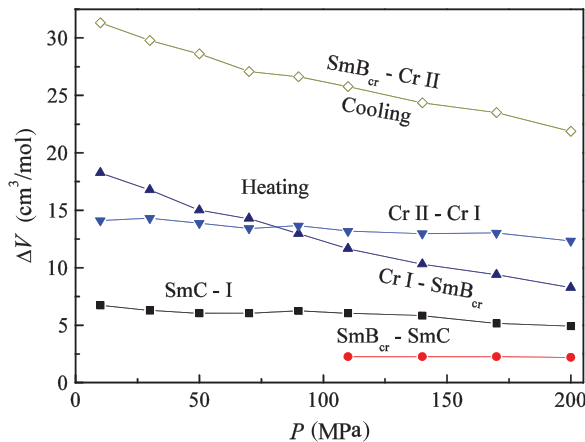


Figure 9. Effect of pressure on the molar volume change at various phase transitions in 10PBO8.

4.2 Analysis of the clearing line

The specific volumes from Figure 2 can be used to determine the interaction parameter Γ in Equation (1). A plot of $\ln(T/T_0)$ vs. $\ln(V/V_0)$ is shown in Figure 10 for the SmC-Iso transition. The (T, V) values for the upper and lower bounds of the step changes in volume give equivalent values, $\Gamma = 2.65 \pm$

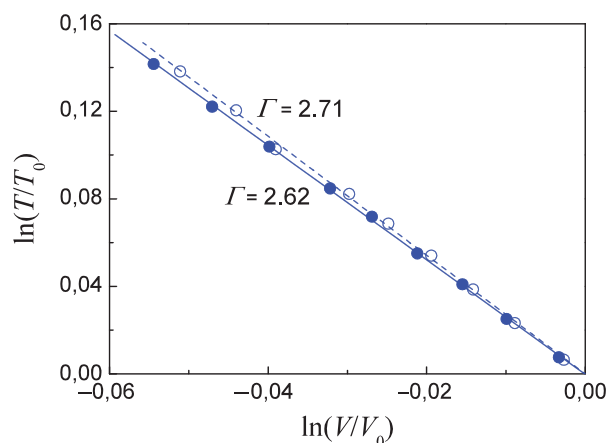


Figure 10. The $\ln(T/T_0)$ vs. $\ln(V/V_0)$ plot for the SmC–Iso transition; from Equation (1) the indicated values of the potential parameter are obtained, corresponding to the respective upper (dashed lines with open circles) and lower lines (solid lines with full circles); T_0 and V_0 represent the values at 0.1 MPa.

0.05. This is close to the Γ reported for other smectogens, whereas the N–Iso transition is usually associated with larger values of Γ (see Table 1). For comparison, included in Table 1 are the potential parameter γ derived from thermodynamic scaling of the longitudinal relaxation times [2, 16, 17, 19, 20, 35–38].

Information on the molecular order of the LC can be gleaned from analysis of the PVT data. The LC–Iso phase change is a first order transition, characterised by an entropy ΔS_{tr} , consisting of two contributions: a constant volume (or configurational) component, $\Delta S_V = \Delta S_{conf}$, and a dilatational part, ΔS_{dil} .

PVT data allow separation of these two contributions [3, 33, 34]:

$$\begin{aligned}\Delta S_{tr} &= \Delta S_{conf} + (\partial S/\partial V)_T \Delta V_{tr} \\ &= \Delta S_{conf} + (\partial P/\partial T)_V \Delta V_{tr}\end{aligned}\quad (2)$$

Combining with the Clausius–Clapeyron equation, $(\partial P/\partial T)_{tr} = \Delta S_{tr}/\Delta V_{tr}$ gives:

$$\Delta S_{conf} = [(\partial P/\partial T)_{tr} - (\partial P/\partial T)_V] \Delta V_{tr}\quad (3)$$

or

$$\begin{aligned}\Delta S_{conf}/\Delta S_{tr} &= [(\partial P/\partial T)_{tr} - (\partial P/\partial T)_V]/(\partial P/\partial T)_{tr} \\ &= 1 - (\partial T/\partial P)_{tr}/(\partial T/\partial P)_V.\end{aligned}\quad (4)$$

In Figure 11 are the isochoric lines derived from the PVT data for the various phases of 10PBO8. The slopes $(\partial T/\partial P)_{tr}$ and $(\partial T/\partial P)_V$ differ considerably, = 0.311 and 0.59 ± 0.05 K/MPa, respectively; this yields the entropy ratio $\Delta S_{conf}/\Delta S_{tr} = 0.47 \pm 0.05$. In Table 1 the entropy ratio values calculated from Equation (4) for several substances are listed. Generally, these entropy ratios are ≤ 0.5 for liquid-like phases and ~ 0.6 – 0.7 for the solid-like SmE phase. The inference is that the entropy change connected with molecular ordering in the N, SmA and SmC phases is roughly half of the total transition entropy, being larger for the more ordered SmE phase.

Table 1. Calamitic LC for which PVT data are available. $\Delta S_{conf}/\Delta S_{tr}$ is the entropy of the Iso–LC transition attributable to conformational disorder. Γ , γ are the interaction potential parameters (see text).

Substance	Phase	T_{cl} (K)	$\Delta S_{conf}/\Delta S_{tr}$	Γ	γ	Ref.
5CB	N	308.3	0.47	5.3	4.1	[6, 16]
6CB	N	301.2	0.32	6.3	4.1	[6, 16]
7CB	N	314.6	0.42	4.7	3.3	[6, 16]
8CB	N	313.8	0.47	4.0	4.2	[6, 16]
3PCH	N	319.5	0.40	5.0		[17]
5PCH	N	328.1	0.46	4.1	3.8	[17]
6PCH	N	322.5	0.45	4.1		[34]
7PCH	N	330.9	0.40	3.3	3.9	[17]
8PCH	N	328.3	0.51	3.4	3.6	[16]
6CHBT	N	316.9	0.49	5.0	5.0	[35]
6OPB8	N	339.2	0.48	2.5	2.7	[36]
6DBT	A	350.1	0.40	2.9	4.0	[13, 38]
10PBO8	C	338.8	0.47	2.65		<i>This work</i>
5BT	E	347.1	0.72	2.2	2.3	[19]
6BT	E	344.2	0.69	2.4	1.9	[19]
7BT	E	345.6	0.74	2.2	2.3	[19]
8BT	E	341.1	0.62	2.7	4.1	[37]

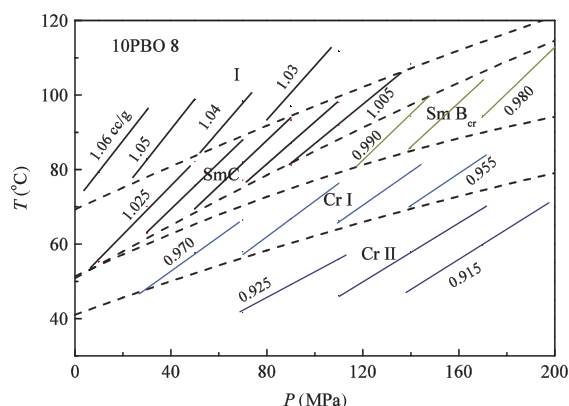


Figure 11. Isochores (solid lines) for all phases of 10PBO8 determined from the PVT results. The specific volumes (in mL g^{-1}) are indicated. Transition lines are denoted by the dashed lines.

5. Conclusions

Combined experiments on 10PBO8 reveal the atypical phase behaviour of this compound. At atmospheric pressure the Cr II–Cr I–SmC–Iso phase sequence occurs on heating, whereas on cooling the Iso–SmC–monotropic SmX–Cr II transitions are observed. Three techniques were employed to identify the X phase: polarising microscopy, the miscibility method and X-ray diffraction. All results are consistent with the SmX being an orthogonal SmB crystalline phase. High-pressure DTA and PVT measurements show that above ca. 15 MPa, the SmB_{cr} phase becomes enantiotropic. With increasing pressure the temperature range of the SmC phase diminishes, and above 350 MPa the phase sequence likely becomes Iso– SmB_{cr} –Cr.

Dielectric studies at ambient pressure quantify the molecular mobility in both smectic phases of 10PBO8. However, observation of the relaxation process was limited to the SmC phase due to masking of the SmB_{cr} dynamics by dc-conductivity. This SmC relaxation, reflecting rotation around the short molecular axis, falls at MHz frequencies, with an activation barrier of 90 kJ mol^{-1} , similar to other liquid-like LC phases [2, 4, 8, 25].

From the equation of state, $V = f(P, T)$, a determination was made of the parameter Γ characterising the steepness of the interaction potential in the SmC phase of 10PBO8. Its value, $\Gamma = 2.65$, is typical for liquid-like LC substances. By comparing the slope of the clearing line, $(\partial T / \partial P)_{\text{tr}}$, with that of the isochoric lines in the SmC phase, $(\partial T / \partial P)_{\text{V}}$, the ratio of the conformational entropy to the total entropy of the SmC–Iso transition was estimated. The obtained value, ratio $\Delta S_{\text{conf}} / \Delta S_{\text{tr}} = 0.47 \pm 0.05$, is typical for clearing

transitions in other liquid-like LC phases, whereas it reaches a value of 0.7 for crystal-like E–I phase transitions.

Acknowledgement

The work at NRL was supported by the Office of Naval Research.

References

- [1] Roland, C.M. *Soft Matter* **2008**, *4*, 2316–2322.
- [2] Urban, S.; Roland, C.M. *J. Non-Cryst. Solids* **2011**, *357*, 740–745.
- [3] Orwoll, R.A.; Sullivan, V.J.; Campbell, G.C. *Mol. Cryst. Liq. Cryst.* **1987**, *149*, 121–140.
- [4] Urban, S.; Würflinger, A. *Adv. Chem. Phys.* **1997**, *98*, 143–216.
- [5] Pollmann, P. High pressure investigations. In *Handbook of Liquid Crystals*: Demus, D.; Goodby, J.; Gray, G.W.; Spiess H.W.; Vill, V., Ed.; Wiley-VCH: Weinheim, 1998; Volume 1, pp. 355–378.
- [6] Würflinger, A.; Sandmann, M. Equation of state for nematics. In *Physical Properties of Liquid Crystals, Nematics, EMIS Datareview Series 25*: Dunmur, D.A.; Fukuda, A.; Luckhurst, G.R., Ed.; Institution of Electrical Engineers: London, 2000; pp. 151–161.
- [7] Würflinger, A.; Urban, S. Dielectric relaxation processes in condensed matter under pressure. In *Relaxation Phenomena*: Haase, W.; Wróbel, S., Ed.; Springer: Heidelberg, 2003; pp. 71–88.
- [8] Urban S.; Würflinger A. Molecular rotations in liquid crystals as seen by the dielectric spectroscopy methods. In *Relaxation Phenomena*: Haase, W.; Wróbel, S., Ed.; Springer: Berlin, 2003; pp. 181–204.
- [9] Chandrasekhar, S.; Shashidhar, R. *Advances in Liquid Crystals*: Brown, G.H., Ed.; Academic Press: London, 1978; Vol. 4, pp. 83–120.
- [10] Urban, S.; Massalska-Arodz, M.; Würflinger, A.; Dabrowski, R. *Liq. Cryst.* **2003**, *30*, 313–318.
- [11] Urban, S.; Czub, J.; Dąbrowski, R.; Würflinger, A. *Phase Trans.* **2006**, *79*, 331–342.
- [12] Maeda, Y.; Urban, S. *Phase Trans.* **2010**, *83*, 467–481.
- [13] Würflinger, A.; Urban, S. *Phys. Chem. Chem. Phys.* **2001**, *3*, 3727–3731.
- [14] Urban, S.; Würflinger, A. *Z. Naturforsch. A* **2001**, *56*, 489–492.
- [15] Roland, C.M.; Hensel-Bielowka, S.; Paluch, M.; Casalini, R. *Rep. Prog. Phys.* **2005**, *68*, 1405–1478.
- [16] Urban, S.; Würflinger, A. *Phys. Rev. E: Stat., Nonlinear, Soft Matter Phys.* **2005**, *72*, 021707 (1–4).
- [17] Urban, S. *Liq. Cryst.* **2011**, *38*, 1147–1152.
- [18] Chandrasekhar S. *Liquid Crystals*, 2nd ed.; Cambridge University Press: Cambridge, UK, 1992.
- [19] Roland, C.M.; Bogoslovov, R.B.; Casalini, R.; Ellis, A.R.; Bair, S.; Rzoska, S.J.; Czuprynski, K.; Urban, S. *J. Chem. Phys.* **2008**, *128*, 224506 (1–9).
- [20] Fragiadakis, D.M.; Urban, S.; Massalska-Arodz, M.; Bogoslovov, R.B.; Czub, J.; Roland, C.M. *J. Phys. Chem. B* **2011**, *115*, 6437–6444.
- [21] Yameshita, M.; Terada, M.; Mori, S.; Katagiri, K. *Eur. Pat. Appl.* 458.347 (27.11.1991).

- [22] Zaschke H., *J. Prakt. Chemie* **1975**, 317, 617–630.
- [23] Zoller, P.; Walsh, D.J. *Standard Pressure–Volume–Temperature Data for Polymers*: Technomic Publications: Lancaster, PA, 1995.
- [24] Urban, S.; Czub, J.; Dabrowski, R.; Würflinger, A. *Phase Trans.* **2006**, 79, 331–342.
- [25] Domenici, V.; Czub, J.; Geppi, M.; Gestblom, B.; Urban, S.; Veracini, C.-A. *Liq. Cryst.* **2004**, 31, 91–99.
- [26] Gray, G.W.; Goodby, J.W.G. *Smectic Liquid Crystals. Textures and Structures*: Leonard Hills: Glasgow, 1984.
- [27] Tykarska, M.; Skrzypek, K. *Phase Trans.* **2007**, 80, 203–207.
- [28] Czupryński, K.; Przedmojski, J.; Baran, J.W. *Mol. Cryst. Liq. Cryst.* **1995**, 260, 435–442.
- [29] Jasiurkowska, M.; Budziak, A.; Czub, J.; Urban, S. *Acta Phys. Polon. A* **2006**, 110, 795–805.
- [30] Jasiurkowska, M.; Budziak, A.; Czub, J.; Massalska-Arodz, M.; Urban, S. *Liq. Cryst.* **2008**, 35, 513–518.
- [31] Dabrowski, R.; Przedmojski, J.; Spadlo, A.; Dziaduszek, J.; Tykarska M. *Phase Trans.* **2004**, 77, 1103–1110.
- [32] Pindak, R.; Moncton, D.E.; Davey, S.C.; Goodby, J.W. *Phys. Rev. Lett.* **1981**, 46, 1135–1138.
- [33] Sandmann, M.; Hamann, F.; Würflinger, A. *Z. Naturforsch. A* **1997**, 52, 739–747.
- [34] Sandmann, M.; Hamann, F.; Würflinger, A. *Z. Naturforsch. A* **1999**, 54, 281–286.
- [35] Bogoslovov, R.B.; Roland, C.M.; Czub, J.; Urban, S. *J. Phys. Chem. B* **2008**, 112, 16008–16011.
- [36] Urban, S.; Roland, C.M.; Czub, J.; Skrzypek, K. *J. Chem. Phys.* **2007**, 127, 094901 (1–6).
- [37] Würflinger A.; Urban S. *Liq. Cryst.* **2002**, 29, 799–804.
- [38] Urban S.; Würflinger, A. *XVI Conference on Liquid Crystals, Stare Jablonki 2005, Conference Proceedings*: Perkowski, P.; Raszewski Z.; Zieliński, J., Eds.; MUT Warszawa, 2007; pp. 177–184 (ISBN 978-83-89399-47-2).